

Prediction of Molecular Distribution and Temperature Profile of FCC Process through Molecular-Level Kinetic Modeling

Zhengyu Chen¹, Gang Wang¹, Suoqi Zhao², and Linzhou Zhang¹

¹China University of Petroleum Beijing

²China University of Petroleum

July 11, 2022

Abstract

This work aims to develop a molecular-level process model framework for simulating the FCC process. The process model consists of the riser, regenerator, and separation models. A complex molecular-level kinetic model, containing 3,652 molecules and 8,202 reactions, was developed for the heavy oil FCC process. The kinetic model was coupled with the riser model, and the model parameter was tuned by a set of systematic experimental data from a pilot-scale plant. After that, a two-zone and two-phase regenerator model was built. The regenerator was combined with the riser model, and the coupled modeling and process simulation for the riser-type FCC unit was developed. The results show that the calculated value of fraction yields and key bulk properties agrees well with the experimental data. Moreover, the molecular distribution of the product and temperature profile was also predicted.

Prediction of Molecular Distribution and Temperature Profile of FCC Process through Molecular-Level Kinetic Modeling

Zhengyu Chen, Gang Wang*, Suoqi Zhao and Linzhou Zhang*

State Key Laboratory of Heavy Oil Processing, Petroleum Molecular Engineering Center (PMEC), China University of Petroleum, Beijing, 102249, P. R. China

Abstract

This work aims to develop a molecular-level process model framework for simulating the FCC process. The process model consists of the riser, regenerator, and separation models. A complex molecular-level kinetic model, containing 3,652 molecules and 8,202 reactions, was developed for the heavy oil FCC process. The kinetic model was coupled with the riser model, and the model parameter was tuned by a set of systematic experimental data from a pilot-scale plant. After that, a two-zone and two-phase regenerator model was built. The regenerator was combined with the riser model, and the coupled modeling and process simulation for the riser-type FCC unit was developed. The results show that the calculated value of fraction yields and key bulk properties agrees well with the experimental data. Moreover, the molecular distribution of the product and temperature profile was also predicted.

Keywords: Fluid catalytic cracking; Molecular-level kinetic model; Riser model; Process simulation;

1. Introduction

The fluid catalytic cracking (FCC) process is a significant technology for converting heavy oil to light fractions (such as LPG, gasoline, and diesel) and producing high-quality gasoline and low-cost olefins. The profitability of refineries is closely dependent on the FCC

product yield and quality. With the increasing trend of crude oil deterioration, the FCC unit is currently facing the challenge of producing lighter products from inferior fossil fuels. In addition to developing the novel FCC technology, building a process model also plays an instrumental and crucial role in the process optimization of the FCC unit.

The kinetic model is the cornerstone for modeling and simulating the FCC process. In the past, due to the limitations of analytical methods and modeling capabilities, lumped kinetic models were frequently used to model the FCC process^{1,2}. The lumped model enables the calculation of the product yield and, to a certain extent, can guide the process optimization³⁻⁶. However, as the demand for the refined management of the refining industry was proposed, the predictive capacity of the lumped model can no longer match the requirements. It is difficult to obtain further the detailed molecular composition and bulk properties of the product. With the development of petroleum refining molecular management, building a kinetic model from the molecular level can successfully overcome the shortcomings of the lumped kinetic model. The molecular-level kinetic model originated in the 1990s and has received wide attention. So far, it has been broadly applied to complex reaction systems, including petroleum, coal, and biomass⁷⁻¹⁶. For the FCC process, according to the molecular details presented in the reaction network, the kinetic model can be classified into two categories: mechanistic-level kinetic model and pathway-level kinetic model. The represented modeling frameworks for the mechanistic-level kinetic model are the single event kinetic model¹⁷ and the bond-electron matrix (BEM)^{18,19}. Watson screened a series of representative molecules in petroleum and used the BEM framework to develop mechanistic-level kinetic models for these molecules^{20,21}. The developed model accurately calculated the yield for the key molecules and captured the

conversion law of hydrocarbon molecules in the catalytic cracking. Subsequently, the mechanistic-level kinetic model was applied to the vacuum gas oil (VGO) fraction. Moustafa et al. used the single event method to develop the kinetic model for VGO FCC at the mechanistic level²². The model obtained the distribution of each fraction and key components along the riser. In addition to the mechanistic-level kinetic model, there were also a large number of studies on molecular-level kinetic models at the pathway level. The most typical frameworks are the structure-oriented lumping (SOL)^{23,24} and the molecular type and homologous series (MTHS) matrix^{25,26}. Two decades ago, Christensen et al. pioneered the application of the SOL framework to the VGO FCC process, and the model can calculate and predict the fraction yield and molecular distribution of product²⁷. Recently, Qin et al. re-used the SOL method to build the molecular-level kinetic model for the heavy oil FCC, and the effect of the riser diameter on the product yield was investigated²⁸. Compared with the kinetic model at the pathway level, the mechanistic-level kinetic model can contain more details of the chemical reaction. However, the complexity of the network is much greater than that of the kinetic model at the molecular level. For the heavy oil FCC process, excessive reaction details will lead the model difficult to solve. To balance the computational time and predictive power of the model, researchers generally use the molecular-level kinetic model at the pathway level to simulate the heavy oil processing.

The molecular-level kinetic model can obtain the conversion law of each molecule in the reaction process, and the molecular composition in the product can also be calculated. However, for adiabatic reactors such as the riser, the heat effects of the reaction process also have an important impact on the reaction rate. Dewachtere et al. proposed a method of coupling the

molecular-level kinetic model with the heat balance equation, and the reaction temperature along the riser was calculated²⁹. Recently, Liu et al. developed an FCC molecular-level kinetic model combined with the feedback of the heat effect based on the SOL framework³⁰. The developed model can accurately calculate the fraction yield and the outlet temperature of the riser.

In addition to the riser, the regenerator is the other core device of the FCC unit. Generally, the regenerator can be divided into the dense bed and freeboard, and the coke burning mainly occurs in the dense bed. In the past decades, a series of regenerator mathematical models have been proposed, such as the homogeneous model³¹, the two-zone and two-phase model³², the three-zone and two-phase model³³, and the three-phase model³¹. Subsequently, Ali et al. coupled the riser model with a two-phase regenerator model and modeled a riser-type FCC unit³⁴. Moreover, Han et al. combined a four lumped model with a two-zone and two-phase regenerator model to build a VGO FCC process model^{35,36}. On this basis, they used the model to simulate the steady-state and dynamic-state behavior of the FCC unit. Recently, Zhou et al. constructed a molecular-level process model for crude oil catalytic cracking to chemicals process based on the Aspen Hysys software platform³⁷. The kinetic model adopted a 21 lumped kinetic model in Hysys software, and the developed model can accurately calculate product yield.

In the previous research, modeling and simulation of the FCC process commonly used the lumped kinetic, and the number of the lumped in the model rarely exceeds 100. The process model is far from the molecular-level³⁸. This work will go deep into the molecular level and develop a molecular-level process simulation framework for the FCC process. The molecular-

level kinetic model was developed based on the FCC reaction mechanism, and coupled with the riser model. On this basis, the regenerator model and molecular-level separation model were built. Finally, the process simulation of a pilot-scale FCC unit was accomplished. The results show that the developed process model can calculate and predict the molecular distribution, fraction yield, key bulk properties of the product, and temperature distribution along the riser. A good agreement between experimental and calculated values was obtained.

2 Experimental and Simulation Overview

Modeling and simulating the FCC unit is a challenging task involving multi-unit coupling. In addition to building a kinetic model and the reactor model based on the process mechanism, it also needs the support of systematic experiment data. Furthermore, a robust model solving algorithm is also extremely significant. Thus, this work consisted of three parts: the acquisition of experimental data, the development of the kinetic model, and the process simulation of the FCC unit. The overview of the whole model framework for the heavy oil FCC is shown in Figure 1. First, a molecular-level kinetic model for heavy oil FCC was built based on the reaction mechanism and coupled with the riser model. After that, a series of FCC experimental data under various process conditions was obtained from a pilot-scale FCC unit. Model parameters were tuned by these experimental data. On this basis, a two-zone and two-phase regenerator model and a molecular-level separation model were developed. The regenerator model was coupled with the riser model, and the steady-state simulation was completed. We used the tuned parameters to calculate and predict the fraction yield, key bulk properties of the product, molecular distribution, and temperature profile. Moreover, the sensitivity analysis is also carried out to explore the effect of process parameters on the product yield.

3. Molecular-Level Kinetic Model

3.1 Computer-aided Representation of Molecules and Reactions

In order to model the complex molecular conversion system, we proposed a hybrid structural unit and bond-electron matrix (SU-BEM) framework to represent petroleum molecules³⁹. According to the characteristics of the petroleum molecular group, we split the oil molecules into 34 structural fragments. After that, a large number of petroleum molecules can be conveniently represented by the combination and splicing of these structural units. The structural units in the SU-BEM framework are shown in Figure 2.

The structural unit is a series of self-defined strings essentially. To link these strings with the chemical-level information, we added the bond-electron matrix, containing molecular connectivity information, into the framework. The bond-electron matrix was mapped to the SUs, as shown in Figure 2. To further explain the automatic generation method of chemical reaction based on the SU-BEM framework, we take the dealkylation reaction as an example. Initially, the reaction rule needs to be programmed. The reaction rule will be used as input to modify the SUs of the reactant, and the SUs of the product molecules can be obtained. After the product SUs are obtained, these SUs will be converted into the bond-electron matrix automatically. According to the molecular connectivity information, the chemical-level information can be obtained, such as the molecular image, physical properties, and chemical properties of molecules. The SU-BEM framework combined the advantage of the SOL and BEM. The modeler can intuitively manipulate the molecular group to describe the chemical reaction. For more complex tasks, such as the chemical bonds change and molecule image generation, they will be delivered to the SU-BEM framework for automatic implementation.

3.2 Feedstock Composition Modeling

Building a computer-based molecular compositional model is the first step in simulating the FCC process at the molecular level. In our previous work³⁹, the compositional modeling of petroleum fraction based on the probability density function (PDF) was developed. The method has been applied to the gasoline, diesel, VGO, and heavy oil fraction³⁹⁻⁴¹. The FCC feedstock is the same as the previous model in this work⁴². The density, elemental analysis, mass spectrometry, and simulated distillation of the heavy oil were used as input to the molecular reconstruction algorithm. Then, the global optimization algorithm (Genetic Algorithm) was called to tune the parameter of the PDFs. When a good agreement between calculated and experimental values was observed, the molecular compositional model of the feedstock can be obtained. The calculated results of the feedstock compositional model are listed in Table S1, which display a good agreement. The results show that the tuned compositional model can capture the bulk properties of the heavy oil, and it can be used as input for subsequent reaction kinetic model.

3.3 Reaction Rule Library and Reaction Network for FCC Process

The reaction rule described the conversion law between reactant and product molecules. Thus, the formulation of the reaction rule needs to follow the reaction mechanism strictly. We have summarized and generalized the reaction mechanism of the FCC process and programmed a reaction rule library for FCC. When building the kinetic model, we can select and call these reaction rules directly from the library to generate the reaction network. The reaction rule and the representative reaction are shown in Figure 3. The library contains 28 reaction rules, including cracking reaction, isomerization, hydrogen transfer, alkylation, polymerization, ring

closure, ring opening, dehydrogenation, hydrogenation, and condensation reaction. Each reaction rule was further divided into the sub-reaction rule according to the molecule type. The constructed reaction rule library can cover the common chemical reactions in the FCC process. Moreover, more details about these reaction rules can be found in our previous work^{42,43}.

After the reaction rule library was obtained, *C7*-tetrahydronaphthalene was selected as an example to validate the reaction rule. Figure 4 exhibits the partial reaction network of the *C7*-tetrahydronaphthalene. As shown in the figure, the reactant molecule first undergoes the ring side chain cracking reaction to generate aromatics and a series of olefins. These olefins molecules can occur a cracking reaction to form the lighter olefins, such as propylene and butene. Besides, these olefins can also undergo hydrogen transfer reaction with the naphthenic ring, and paraffins and aromatics can be obtained. The generated paraffins will continue to undertake the cracking reaction to produce the olefins with a low carbon number. For aromatics, they will undergo the dehydrogenation and condensation reaction to generate polycyclic aromatic hydrocarbons (PAH). According to the reaction network of *C7*-tetrahydronaphthalene catalytic cracking, it was found that the automatically generated reaction network is matched to the conversion law of the FCC process. On this basis, we applied the reaction rule to the heavy oil molecules in the compositional model, and the FCC reaction network, containing 3,652 molecules and 8,202 reactions, was eventually generated.

3.4 Kinetic Model and Catalyst Deactivation Model

3.4.1 Kinetic Model for the FCC

After obtaining the reaction network, we extracted the conversion relationship between the reactant and product molecules from the network. Subsequently, the conversion relationship

was automatically converted to the reaction rate expression base on an in-house algorithm.

Since the FCC process is a heterogeneous catalytic reaction system, the reactant molecules will first absorb into the catalyst surface and undergo the FCC reaction. The generated product molecules are desorbed and returned to the gas phase. In order to describe the physical and chemical changes on the catalyst, we selected the Langmuir-Hinshelwood-Hougen-Watson (LHHW) model as the kinetic model, as shown in Eq. (1). The surface reaction rate in equation (1) can be calculated using the Arrhenius equation, as shown in Eq. (2)

$$r_j = \frac{k_{srj} K_{ads_A} K_{ads_B} (C_A^m C_B^n)}{1 + \sum K_{ads_i} C_i} \quad (1)$$

$$k_{srj} = A_j e^{-\frac{E_{aj}}{RT}} \quad (2)$$

The FCC process is a complex molecular conversion system involving thousands of molecules and reactions. It is difficult to directly tune the model parameter (pre-exponential factor, activation energy, and adsorption constant) using the experimental data. To reduce the parameter tuned in the model, we used the linear free energy relationship (LFER) and quantitative structure-reactivity correlations (QSRCs) to minimize the model parameter to a manageable range. In our previous work⁴², the LFER and QSRCs were discussed and more details can be found in the supporting information.

3.4.2 Catalyst Deactivation Model

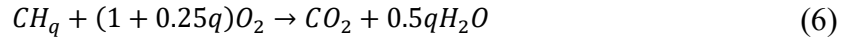
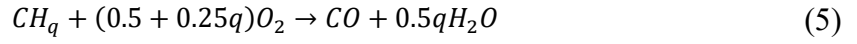
As the reaction proceeds, a large amount of coke is formed during the FCC process. The generated coke adsorbs on the catalyst, resulting in a lower reaction rate. In this work, the functions of coke adsorption and basic nitrogen poisoning were used to describe the effect of the coke content and basic nitrogen on reaction rate, respectively, as shown in Eq. (3) and (4).

$$\varphi_{ck} = (1 + \alpha C_{ck})^{-\beta} \quad (3)$$

$$f_N = \frac{1}{1 + k_N W_N \frac{t_c}{CTO}} \quad (4)$$

3.5 Coke Burning Kinetic Model

The coke attached to the catalyst is a complex mixture containing many PAHs. It is a challenging task to obtain its detailed molecular composition. This work assumes that the average chemical formula of coke is CH_q , and reaction equations of coke burning in the regenerator were shown in Eq. (5) - (8)⁴⁴⁻⁴⁶. Eq. (5) and (6) are for coke combustion, while Eq. (7) and (8) are for carbon monoxide oxidation.



The kinetic model for coke burning is shown in Eq. (8) – (11), and the kinetic parameters can be found in Table S2.

$$r_{RG1} = k_{RG1}^* C_{ck} C_{O_2} \quad (8)$$

$$r_{RG2} = k_{RG2}^* C_{ck} C_{O_2} \quad (9)$$

$$r_{RG3} = k_{RG3} C_{CO} C_{O_2}^{0.5} C_{H_2O}^{0.5} \quad (10)$$

$$r_{RG4} = k_{RG4} C_{CO} C_{O_2}^{0.5} \quad (11)$$

$$k_{RG1}^* = \frac{k_{RG1}}{1 + \sigma} \quad (12)$$

$$k_{RG2}^* = \frac{k_{RG1} \sigma}{1 + \sigma} \quad (13)$$

4 Riser and Regenerator Model

4.1 A Pilot-scale FCC Unit

We can calculate the reaction rate of each molecule based on the kinetic model. However,

for modeling the FCC process, we also need to focus on the mass and heat transfer during the reaction process. Therefore, it is necessary to develop the corresponding reactor model.

We developed an FCC process model and applied it to a pilot-scale FCC plant. The modeling and experimental scheme are shown in Figure 5. Compared with the traditional pilot plant, the pilot-scale FCC unit in this work was improved. The feedstock can be injected from three different locations into the riser to obtain the product distribution at the different positions of the riser. The main process parameters of the riser were listed in Table S3 in the supporting information. The experimental process is as follows:

The heavy oil was preheated and pumped into the riser to contact the catalyst from the regenerator. The feedstock was vaporized, and the catalytic cracking reaction occurred. The gaseous product was separated from the top of the disengager. After that, the gaseous component was cooled. The gas was fed into the gas chromatography, while the liquid was cut into gasoline, diesel, and slurry oil by the distillation device. The spent catalyst was delivered to the regenerator and underwent the coke-burning reaction with oxygen. The generated stack gas was discharged from the top of the regenerator, while the regenerated catalyst was recycled back to the riser to enable continuous operation of the plant. The detailed experimental conditions are listed in Table S4. The process conditions in Table S4 were designed in terms of the industrial FCC unit. It is capable of covering typical process conditions for heavy oil FCC.

4.2 Riser Model

The process simulation for the FCC is mainly divided into two parts: the riser and regenerator. The riser is an adiabatic reactor. The riser model contains the feedstock vaporization, mass balance, and heat transfer between gas and solid phases. The modeling

diagram of the riser is shown in Figure 5. To accurately describe the physical and chemical changes in the riser, the riser model was divided into the vaporization section and reaction section.

4.2.1 Feed Vaporization Section

The liquid feedstock, preheated by the preheater, will be instantly vaporized when it contacts the high-temperature catalyst. The vaporization model is used to calculate the temperature of the gas and solid phases after vaporization. Since the vaporization is completed instantaneously, the gas phase reaches a saturated state. Thus, we assumed that there was no chemical reaction in the vaporization section³⁵. According to the above assumption and heat balance equation, the catalyst temperature of the vaporization section outlet can be derived, as shown in Eq. (14).

$$T_c^{vap} = T_c^{in} - \frac{F_o}{F_c C_{p,c}} \left[C_{p,l} (T_o^{vap} - T_o^{in}) + \frac{F_s C_{p,s}}{F_o} (T_o^{vap} - T_s^{in}) + \Delta H_{vap,oil} \right] \quad (14)$$

The vaporization enthalpy of the oil in Eq. (14) can be calculated using Eq. (15).

$$\Delta H_{vap,oil} = 0.3843 T_{MeABP} + 1.0878 \times 10^3 \exp\left(\frac{-M_w}{100}\right) - 98.153 \quad (15)$$

Since the gas phase is the saturated state, the gas temperature of the vaporization outlet can be estimated using the Antoine equation (Eq. (16)). The details of the parameter regression for the Antoine equation can be found in the supporting information.

$$T_o^{vap} = \frac{B}{A - \log(P \times y_o)} - C \quad (16)$$

$$y_o = \frac{F_o}{F_o + F_s} \quad (17)$$

4.2.2 Reaction Section

In this work, we assumed that the flow regime of the gas and solid phase in the riser is

plug flow. It is because the riser diameter is 16 mm, and the relatively small reactor diameter allows us to ignore the radial concentration and temperature distribution in the riser. According to the model proposed by Froment et al.²⁹, the mass balance equation for the gaseous phase can be derived, as shown in Eq. (18).

$$\frac{dC_i^{RS}}{dz_{RS}} = \frac{\rho_c \varepsilon_c^{RS}}{v_o^{RS}} R_i \varphi_{ck} \quad (18)$$

φ_{ck} is the catalyst deactivation function of coke, as shown in Eq. (3). ε_c^{RS} and ε_o^{RS} are the volume fractions of catalyst and oil phase, respectively.

$$\varepsilon_c^{RS} = \frac{F_c}{v_c^{RS} \rho_c A_{RS}} \quad (19)$$

$$\varepsilon_o^{RS} = 1 - \varepsilon_c^{RS} \quad (20)$$

Furthermore, the temperature distribution in the riser can be calculated by the heat balance equation of the gas-solid phase, as shown in Eq. (21) and (22). The parameters used in Eq. (21) and (22) are listed in the supporting information.

$$\frac{dT_c^{RS}}{dz_{RS}} = \frac{A_{RS} h_p A_p}{F_c C_{p,c}} (T_o^{RS} - T_c^{RS}) \quad (21)$$

$$\frac{dT_o^{RS}}{dz_{RS}} = \frac{A_{RS}}{F_o C_{p,g}} \left[h_p A_p (T_c^{RS} - T_o^{RS}) + \rho_c \varepsilon_c^{RS} \sum_j (-\Delta H_j r_j) \right] \quad (22)$$

4.3 Regenerator Model

The regenerator is a fluidized bed reactor, but the flow regime of the gas-solid phase is different from the riser. In general, the regenerator is separated into the dense bed and the freeboard. There are a large number of spent catalysts in the dense bed, and the dense bed is again divided into the bubble phase and emulsion phase, as shown in Figure 5.

4.3.1 Dense Bed Model

The dense bed model in this work adopts the classical two-phase (bubble phase and

emulsion phase) theory³¹. Oxygen in the bubble phase must overcome the mass transfer resistance and enter the catalyst surface for coke burning. At the same time, the generated stack gas also needs to overcome the mass transfer resistance and return to the bubble phase. According to previous studies³⁴, the bubble phase and emulsion phase can be regarded as the plug flow reactor (PFR) and continuous stirred tank (CST), respectively. In other words, the coke content and the reaction temperature remain unchanged. They are the same as the outlet of the dense bed, while there is a concentration gradient for the stack gas composition.

We can derive the mass balance equations of stack gas molecules in the emulsion phase and the bubble phase based on the above discussion, as shown in Eq. (23) and (24)⁴⁷.

$$v_{g,E}^D \frac{dC_{i,E}^D}{dz_{RG}} = \frac{K_I}{\varepsilon_{g,E}^D} (C_{i,B}^D - C_{i,E}^D) + R_{i,E}^D \quad (23)$$

$$v_{g,B}^D \frac{dC_{i,B}^D}{dz_{RG}} = \frac{K_I}{\varepsilon_{g,B}^D} (C_{i,E}^D - C_{i,B}^D) + R_{i,B}^D \quad (24)$$

Eq. (23) and (24) can be divided into two parts. One is for mass transfer rate, and the other is for reaction rate. The correlations of parameters and properties for mass balance and the reaction rate expression of the stack gas were described in the supporting information.

According to Eq. (23) and (24), the concentration distribution of each molecule in the emulsion and bubble phase can be calculated. After that, the average concentration distribution of each species in the dense bed can be calculated by Eq. (25).

$$C_i^D = \frac{C_{i,E}^D v_{g,E}^D \varepsilon_{g,E}^D + C_{i,B}^D v_{g,B}^D \varepsilon_{g,B}^D}{u_g} \quad (25)$$

Since the emulsion phase is a CST, the concentration of coke on the regenerated catalyst can be deduced according to the mass balance equation, as shown in Eq. (26).

$$C_{ck}^D = C_{ck}^{RS} - \frac{M_{wck}}{0.5q\rho_g F_c} (F_{air} C_{H_2O}^{in} - F_{air} C_{H_2O}^D) \quad (26)$$

Moreover, according to the heat balance equation (Eq. (27)), the dense bed temperature can be calculated iteratively.

$$F_c(H_c^{RS} - H_c^D) + F_{air}(H_{air}^{in} - H_g^D) + Q_{re}^D = 0 \quad (27)$$

The reaction heat can be calculated using Eq. (28), and the enthalpy of each substance and stream was listed in Table S6.

$$Q_{re}^D = \frac{1}{\rho_g} \sum_i (F_{air} C_i^{in} - F_{air} C_i^D) \Delta H_{f_i} + \frac{1}{0.5q\rho_g} (F_{air} C_{H_2O}^{in} - F_{air} C_{H_2O}^D) \Delta H_{f_{ck}} \quad (28)$$

4.3.2 Freeboard Model

The catalyst in the dense bed flows upward with bubbles. Bubbles burst on top of the dense bed, and a small number of catalysts are carried into the freeboard. The modeling schematic of the freeboard is shown in Figure 5. In this work, the freeboard is treated as a PFR. Thus, the mass balance equation of molecules and coke can be derived based on the PFR model, as shown in Eq. (29) and (30), respectively³⁵.

$$\frac{u_g}{\varepsilon_g^F} \frac{dC_i^F}{dz_{RG}} = -\frac{\rho_c \varepsilon_c^F (r_{RG1}^F + r_{RG2}^F)}{\rho_g \varepsilon_g^F} C_i^F + R_i^F \quad (29)$$

$$\frac{u_c^F}{\varepsilon_c^F} \frac{dC_{ck}^F}{dz_{RG}} = -(r_{RG1}^F + r_{RG2}^F) \quad (30)$$

Besides, the temperature distribution in the freeboard can be obtained by the heat balance equation³⁵, as shown in Eq. (31). The correlations of properties and rate equations used in the freeboard were also shown in the supporting information.

$$(u_c^F \rho_c C_{p,c} + u_g \rho_g C_{p,g}) \frac{dT^F}{dz_{RG}} = Q_{re}^F \quad (31)$$

$$Q_{re}^F = \rho_c \varepsilon_c^F \left(\frac{r_{RG1}^F \Delta H_{RG1}}{M_{wck}} + \frac{r_{RG2}^F \Delta H_{RG2}}{M_{wck}} + r_{RG4}^F \Delta H_{RG4} \right) + \varepsilon_g^F r_{RG3}^F \Delta H_{RG3} \quad (32)$$

4.4 Product Separation Model

The liquid product from the riser was sent to the distillation device, and the liquid fraction

was split into gasoline, diesel, and slurry oil. In the traditional molecular-level separation model, the molecule was separated based on boiling point, and there was no overlap between fractions. It means that each molecule can only enter one fraction. However, it is difficult to ensure that each molecule was cut clearly for the pilot-scale or industrial distillation process. To simulate the distillation process at the molecular level, we introduced a separation efficiency factor to describe the overlap between fractions⁴⁸.

Separation efficiency is calculated using the modified Sigmoid function, as shown in Eq. (33). It is an S-shaped curve function. When the independent variable, T_{bp} , approaches positive infinity or negative infinity, the function value approaches 1.

$$\vartheta = 1 - \frac{1}{1 + e^{-a(T_{bp}-b)}} \quad (33)$$

Where b represents the cutting point, and a is the parameter for separation efficiency. If a decreases, the overlap interval between fractions is larger. The effect of the parameter variation on the separation efficiency was explored, as shown in Figure S2.

After obtaining the efficiency factor of each molecule, we can deduce the mole fraction of molecules in each fraction.

$$y_i^f = \vartheta y_i^* \quad (34)$$

$$y_i^b = y_i^* - y_i^f \quad (35)$$

4.5 Solution Strategy for Molecular-level FCC Process Model

There was a strong coupling between the riser and regenerator when the FCC process model was developed. The direction and connection sequence of each stream in the model are shown in Figure 5. To make the FCC process model converge, it is necessary to ensure the mass and heat balance between the riser and the regenerator. It means that the coke content on

the regenerated catalyst is consistent with that of the initial input to the riser. Besides, the regenerated catalyst temperature should also be the same as that of the input to the riser. The iteration scheme of the FCC process model is shown in Figure 6(a). The detailed calculation process is as follows:

We first need to input the heavy oil stream information, such as molecular composition and oil temperature, and assign the initial values for the catalyst temperature and the coke content on the catalyst. Oil and catalyst streams were delivered into the vaporization model to calculate the temperature of the catalyst and gaseous phase after the vaporization. After that, the gas and solid streams were automatically input into the reaction model. The molecular-level kinetic model will be called to calculate the molecular composition of the product, spent catalyst temperature, and coke content on the spent catalyst. The spent catalyst stream will be linked to the regenerator model, and the coke burning reaction will occur in the regenerator. Subsequently, the regenerated catalyst temperature and coke content on the regenerated catalyst can be calculated, and the error between the calculated and initial value can also be obtained. If the error exceeds the convergence tolerance, the secant method will be called to tune the initial value. Next, according to the above process, repeated iteration until the model converged. Once the model converges, the gaseous composition at the riser outlet will be delivered into the molecular-level separation model to obtain the yield and composition of each fraction.

According to the above model convergence algorithm, the molecular-level kinetic model needs to be solved for each iteration. For the complex molecular reaction system coupled with gas-solid phase heat transfer, the kinetic model is difficult to solve in a short time. It is because a strong coupling between mass balance and heat balance results in a sharp increase in

computational time. To reduce the computational time of the FCC process model, we adopted a mass-temperature decoupled discretization strategy to solve the molecular-level kinetic model⁴⁹. The schematic diagram of the discretization strategy is shown in Figure 6(b). The strategy separated the entire reactor model into a series of discrete nodes. Each node was assumed to be an isothermal reactor model, and only the mass balance was carried out to obtain the molecular composition of the node outlet. After that, the node temperature difference can be estimated according to the inlet-outlet molecular composition of the node. On this basis, the reaction temperature at the outlet of each node can be obtained. After using the discretization strategy, the differential equation of the heat balance in the riser model can be replaced by the difference equation. The coupling between the mass balance and heat balance was also removed cleverly. Eq. (36) and (37) display the discretized gas and solid heat balance equation, respectively.

$$\Delta T_c^{RS} = \frac{A_{RS} h_p A_p}{F_c C_{p,c}} (T_o^{RS} - T_c^{RS}) \Delta z_{RS} \quad (36)$$

$$\Delta T_o^{RS} = \frac{A_{RS}}{F_o C_{p,g}} \left[h_p A_p (T_c^{RS} - T_o^{RS}) + \rho_c \varepsilon_c^{RS} \sum_j (-\Delta H_{r,j} r_{ij}) \right] \Delta z_{RS} \quad (37)$$

Furthermore, the gas-solid temperature at the outlet of each discrete node can also be deduced, as shown in Eq. (38) and (39).

$$T_{c,i+1}^{RS} = T_{c,i}^{RS} + \Delta T_c^{RS} \quad (38)$$

$$T_{o,i+1}^{RS} = T_{o,i}^{RS} + \Delta T_o^{RS} \quad (39)$$

After applying the strategy to the riser model, we further validated this method. The number of discrete nodes is set to 50, and the product yield and gas-solid phase temperature along the riser are shown in Figure S3. Dots stand for the discretization model, while lines

stand for the rigorous model. As seen from the figure, the calculated results of the two models have an excellent agreement. However, the computational speed was accelerated about 60 times, and the computational time was less than 1 minute by using the decoupled discretization strategy. The results indicate that the computational time of the FCC process simulation can be significantly reduced when the discretization strategy was used. Besides, the solution strategy of the regenerator was discussed in supporting information, as shown in Figure S4.

4.6 Model Parameter Regression

The molecular-level process model for the FCC unit was developed. However, before simulating the FCC process, it is necessary to obtain the kinetic parameter of the molecular-level kinetic model. In our previous work⁴², the molecular-level kinetic model for heavy oil FCC was built, and the model parameter was tuned by five sets of experimental data under different process conditions. On this basis, we selected 13 sets of data under different process conditions to re-tune the model parameters⁵⁰. The process conditions and the initial range of the model parameter (parameters in LFER and QSRCs) were input into the genetic algorithm (GA). After that, the GA will generate multiple sets of model parameters, and the molecular composition of the product and temperature distribution of the riser can be calculated. The molecular composition was delivered into the separation model to calculate the fraction yield and bulk property. The absolute error of the experimental data and the calculated value will be used as the objective function value. Then, the value was passed back to the GA and the model parameter was tuned again. When the objective function value minimized, the tuned parameter can be obtained. The parity plot comparing experimental and calculated value was shown in Figure 7 and a good agreement was observed. Moreover, compared with previous model, the

tuned model can not only be applied to different process conditions, but also adapt to the variation of riser height.

5 Simulation Result and Sensitivity Analysis

5.1 Molecular Distribution and Temperature Profile of Riser

The results of Figure 7 indicate that the fraction yield and reaction temperature of the riser out can be calculated. To further validate the robustness of the parameter, we investigated the effect process condition on the product yield, and the calculated result is shown in Figure 8. The dot is experimental data, and the line is calculated data. The result shows that the yield of the liquefied gas (LPG) and gasoline increases, while the yield of diesel and heavy oil decreases with the rise of the catalyst to oil ratio (CTO). It is because the increase of the CTO leads to an increase in the reaction site. More hydrocarbon molecules come into contact with the catalyst, and the cracking reaction is enhanced. When the riser height increases, the LPG and gasoline yields also increase. It is due to the increase in reaction time. Moreover, as can be seen from Figure 8(c), as the reaction temperature increases, the cracking rate accelerates and the LPG yield improves. In general, the conversion law calculated by the model agrees with the experimental measurement when the reaction condition varies. It also further validates the reliability of the model parameter.

In addition to fraction yield, the temperature distribution along the riser also plays an essential role in obtaining the FCC reaction law. We explored the effect of the reaction condition and riser height on gas-solid phase temperature distribution, as shown in Figure 9. The results show that the calculated value has a great agreement with the experimental data. The calculated temperature distribution also agrees with the past published studies^{36,51,52}. In the

vaporization section, the heavy oil was vaporized after absorbing the heat of the regenerated catalyst and the catalyst temperature decreased. After that, the gas and solid phase enter the reaction section, and the cracking reaction occurs. The calculated results show that the FCC process is an endothermic reaction. Moreover, With the progress of the reaction, the temperature of the gas-solid two phases gradually decreased and finally approached the same temperature at the riser outlet.

Figures 8 and 9 show the effect of reaction conditions on fraction yield and reaction temperature, respectively, and the model parameter was validated. After that, we simulated the pilot-scale FCC unit based on the process condition of experiment 14. When the model converged, the molecular distribution, fraction yield, key bulk property of the product, and temperature distribution were predicted, as shown in Figures 10 and 11. Figure 10 represents the distillation curve and molecular composition for the feedstock and product. As can be seen from Figures 10(a) and (b), the distillation curve of the liquid component is significantly lower than that of the feedstock. It means that a large number of heavy oil fractions are cracked to light fractions, such as gasoline and diesel. Furthermore, the distillation curves of the gasoline, diesel, and slurry oil were represented in Figure 10(b). There is a specific overlapping area between the fractions based on the separation efficiency factor method. The results can better match the experimental phenomena of distillation. Figure 10(c) compares the carbon number distribution of the feedstock and gas and liquid products. For the heavy oil, the carbon number distribution mainly ranges from 20 and 70, with a peak of about 40. After the FCC, many molecules with low carbon numbers are generated, and the molecules are mainly distributed in LPG and gasoline fractions.

After the molecular composition of the product was obtained, the product was divided into several fractions such as dry gas, LPG, gasoline, diesel, and slurry oil based on the molecular-level separation model. The key bulk properties of each fraction and gas-solid phase temperature along the riser were predicted, as shown in Figure 11. As can be seen from the figure, the yield of LPG, gasoline, and diesel gradually increased as the reaction proceeded. The results are agreed well with the published studies⁵¹. It indicates that the developed process model can predict the product distribution pattern. On this basis, the gasoline and diesel hydrocarbon composition was predicted, and the model can capture the composition of key fractions. To further validate the predictive capability of the molecular-level process model, the carbon number distribution in gasoline and LPG was predicted. The comparison of calculated and experimental values is shown in Figures 11(e) and (f). There is a good agreement between experimental measurement and predicted value. The results indicate that the molecular-level process model has stronger predictive power and can obtain more product information than the lumped model.

5.2 Stack Gas Composition and Regenerator Temperature

In addition to the riser model, the calculated result of the regenerator model also plays an essential role in the convergence of the FCC process model. The simulated results of the regenerator are shown in Figure 12 when the whole process model converges. The stack gas composition is shown in Figure 12(a). The results show that the calculated value has a great agreement with the experimental data at the regenerator outlet. Figure 12(b) and (c) show the coke content on the catalyst and the temperature distribution in the regenerator, respectively. Since the emulsion phase in the dense bed is a CST model, there is no concentration or

temperature gradient in the dense bed. For the freeboard, due to the slight after-burning reaction, it led to a decline in coke content and a rise in the temperature of the catalyst. Moreover, according to the experimental result, the coke content on the regenerated catalyst is no more than 0.05 wt%, and the calculated value is also within the experimental range.

5.3 Sensitivity Analysis of Operating Conditions and Riser Geometry

The molecular-level process model for the heavy oil FCC process was developed. To further explore the conversion law of the FCC process, we performed a series of sensitivity analysis on the process model. We first discussed the effect of feedstock composition on product yields, as shown in Figure 13. Figure 13(a) is for the variation of the feedstock component. We sequentially separated paraffins, naphthenes, and aromatics from the feedstock. These components were separately delivered into the FCC process model, and the product yield was calculated. It can be seen from the figure that LPG and gasoline yields are the highest when paraffins are feedstock, followed by naphthenes and aromatics. When paraffins and naphthenes are used as feedstocks, the contents of LPG and gasoline are higher than those of heavy oil. Therefore, it can be speculated that saturated hydrocarbons are high-quality feedstocks for the FCC process or even catalytic cracking for the light olefin process. For the aromatics as feedstock, the generated light fraction is less than the heavy oil FCC, and a large amount of coke will be generated. It indicates that aromatics are not suitable for the FCC. For the oil with high aromatic content, it is recommended to saturate some aromatics by the hydrotreating process before the FCC. In addition to varying the feedstock molecular structure, we also tried to vary the boiling point (BP) distribution of the feedstock to predict the product yield, as shown in Figure 13(b). The lighter the feedstock, the higher the conversion of the feedstock and more

LPG and gasoline available. Moreover, as the boiling point of the fraction increases, the coke content also gradually increases.

In addition to exploring the effect of feedstock composition on the fraction yield, the reaction conditions also have an important impact on the product yield. The effect of the CTO and reaction temperature on the critical fraction is shown in Figure 14. With the growth of the CTO, the yield of LPG, gasoline, and diesel showed an increasing trend. For the LPG, the increase in temperature also leads to a rise in LPG yield. However, for the gasoline fraction, if the CTO is relatively high, the gasoline yield decreases with increasing reaction temperature. It is because the over-cracking of gasoline produces more LPG. When the CTO is relatively low, there is an optimum in the gasoline yield as the temperature varies, around 530 °C. For the diesel fraction, the increase in reaction temperature speeds up the cracking reaction rate, resulting in more diesel cracking to lighter fractions.

Besides, the effect of the CTO and the riser height on the key fraction yield was investigated, as shown in Figure 15. As can be seen from the figure, as the riser height increases, the LPG yield continues to rise. The gasoline fraction increases sharply at the beginning of the reaction and then remains almost constant, while the diesel yield has a maximum value. It is mainly because more and more diesel molecules are cracked into LPG and gasoline fractions as the reaction time increases. For the gasoline fraction, the consumption rate of the gasoline is almost the same as the formation rate. Thus, the gasoline yield is in dynamic equilibrium. It can also be found that the consumption rate of diesel and the generation rate of LPG and gasoline increased obviously with the CTO growth. The calculated results also match the conversion law of the FCC. Furthermore, the effect of the reaction temperature and riser height

on key fraction yield was also calculated, as shown in Figure S5 in the supporting information.

We have discussed the effect of the feedstock composition and reaction condition on the product yield. On this basis, the influence of the riser structure on the product yield was further investigated, and the calculated results are shown in Figure 16. We expanded the riser diameter and discussed the effect of expanding position on product yield and reaction temperature. As the diameter of the riser enlarges, the LPG and gasoline yields gradually increase, while the diesel yield and the outlet temperature of the riser decrease progressively. It is because the variation of the riser diameter affects the gaseous phase velocity. The riser diameter increases, while the gaseous phase velocity declines. It leads to an increase in reaction time, and the light fraction yield also rises. In addition, as the reaction time grows, the cracking depth increases, leading to a decrease in the outlet temperature. For the expanding position, if the expanding position is closer to the bottom of the riser, the light fraction (LPG and gasoline) will increase. It is also because the reaction time increases.

For the whole FCC unit, the flow rate of the air stream has an impact on the quality of the regenerated catalyst. Thus, the effect of the air flow rate for coke burning on stack gas composition and coke content was discussed, as shown in Figure 17. As the air flow increases, the oxygen content in the top of the regenerator gradually rises, while the content of water and CO₂ progressively decreases. Moreover, the coke content on the catalyst also showed a downward trend. The increase of oxygen concentration is beneficial to the combustion of coke. However, as the air flow rate increases, the coke content on the catalyst also tends to be nearly constant. When the flow rate of the air stream is 4 kg/h, a catalyst with excellent cracking performance is obtained.

6 Conclusion

In this work, a molecular-level process model framework for the FCC process was developed. The entire model was centered on a molecular-level kinetic model of the FCC. On this basis, the riser model, the regenerator model, and the molecular-level separation model were built successively. First, a series of reaction rules for the FCC are formulated based on the FCC reaction mechanism. A reaction rule library including 28 rules was obtained. The molecular composition of the heavy oil and reaction rules were used as input, and a reaction network, containing 3,652 molecules and 8,202 reactions, was generated. After that, the reaction network was converted into the rate equation and coupled with the riser model. The model parameter was tuned by 13 sets of experimental data from the pilot-scale plant. On this basis, we combined the riser model with the regenerator model and simulated the heavy oil FCC process. When the process model converged, the molecular distribution, fraction yield, key bulk property, and gas-solid phase temperature profile were predicted. Finally, a sensitivity analysis was performed using the process model. The effects of feedstock composition, process conditions, and reactor structure on the yield of key products were investigated, and the heavy oil FCC reaction law was discussed.

Nomenclature

A = Surface Area, m^2

A_j = Arrhenius constant of reaction j

A_p = Effective interface heat transfer area per unit volume, m^2/m^3

C_{ck} = Weight percentage of coke on the catalyst, wt%

C_i = Concentrations of species i , $kmol/m^3$

C_p = Heat capacity, J/(g·K)

E_{a_j} = Activation energy of reaction family j , kJ

f_N = A catalyst deactivation function of basic nitrogen poisoning

F = Mass flow rate, kg/s

h_p = Interface heat transfer coefficient between catalyst and gas phases, kg/ m²·s

H = Specific enthalpy, kJ/kg

k_N = Parameter for deactivation function of basic nitrogen poisoning

k_{sr_j} = Surface reaction rate constant of reaction j

K_{ads_i} = Adsorption constant of species i

K_l = Interchange coefficient between the bubble phase and emulsion phases, 1/s

M_w = Average molecular weight, g/mol

P = Reaction pressure, kPa

q = Hydrocarbon to carbon atomic ratio in coke

Q_{re} = Reaction heat, kJ/s

r_j = Reaction rate of reaction j

R = Universal gas constant, J/mol·K

R_i = Reaction rate of species i

t_c = Catalyst residence time, s

T = Reaction temperature, K

T_{MeABP} = Mean average boiling temperature for oil, K

u = Superficial velocity, m/s

v = Interstitial velocity, m/s

w_N = Weight percentage of basic nitrogen on the catalyst, wt%

y_o = Mass fraction of oil

y_i^* = Mass fraction in the product for species i

y_i^b = Mass fraction in the back cut for species i

y_i^f = Mass fraction in the front cut for species i

z = Reactor height, m

Greek letters

α, β = Catalyst deactivation parameters

ΔH_f = Heat of formation, kJ/kmol

ΔH_j = Enthalpy of reaction j , kJ/kmol

$\Delta H_{vap,oil}$ = Heat of vaporization of liquid feedstock, kJ/kg

ΔT = Temperature difference, K

Δz = The length of discrete node, m

ε = Volume fraction

ϑ = Separation efficiency

φ_{ck} = A catalyst deactivation function of coking

ρ = Density, kg/m³

σ = Intrinsic CO₂/CO molar ratio

Superscripts

D = Dense bed

F = Freeboard

in = Feed stream

m = Stoichiometry of reactant A

n = Stoichiometry of reactant B

RS = Riser

vap = Vaporization section in the riser

Subscripts

air = Air stream

bp = Boiling point

B = Bubble phase

c = Catalyst stream

ck = Coke

E = Emulsion phase

g = Stack gas stream

o = Oil stream

RG = Regenerator

RS = Riser

s = Steam stream

Author Information

*Corresponding Author Email: Wanggang@cup.edu.cn (G. Wang); lzz@cup.edu.cn (L. Zhang)

Acknowledgments

This work was supported by the National Key R & D Program of China (2021YFA1501201). The authors declare no competing financial interests.

Supporting Information

The additional information on the FCC process model was summarized, which can be found in supporting information.

Reference

1. Jacob SM, Gross B, Voltz SE, Weekman Jr VW. A lumping and reaction scheme for catalytic cracking. *AIChE Journal*. 1976;22(4):701-713.
2. John YM, Patel R, Mujtaba IM. Maximization of Gasoline in an Industrial Fluidized Catalytic Cracking Unit. *Energy & Fuels*. 2017;31(5):5645-5661.
3. Jarullah AT, Mujtaba IM, Wood AS. Kinetic model development and simulation of simultaneous hydrodenitrogenation and hydrodemetallization of crude oil in trickle bed reactor. *Fuel*. 2011;90(6):2165-2181.
4. Jarullah AT, Mujtaba IM, Wood AS. Kinetic parameter estimation and simulation of trickle-bed reactor for hydrodesulfurization of crude oil. *Chemical Engineering Science*. 2011;66(5):859-871.
5. John YM, Patel R, Mujtaba IM. Effects of compressibility factor on fluid catalytic cracking unit riser hydrodynamics. *Fuel*. 2018;223:230-251.
6. Palos R, Rodríguez E, Gutiérrez A, Bilbao J, Arandes JM. Cracking of plastic pyrolysis oil over FCC equilibrium catalysts to produce fuels: Kinetic modeling. *Fuel*. 2022;316:123341.
7. Pereira de Oliveira L, Verstraete JJ, Kolb M. A Monte Carlo modeling methodology for the simulation of hydrotreating processes. *Chemical Engineering Journal*. 2012;207-208:94-102.
8. Schweitzer J-M, Galtier P, Schweich D. A single events kinetic model for the hydrocracking of paraffins in a three-phase reactor. *Chemical Engineering Science*. 1999;54(13-14):2441-2452.
9. Tian L, Shen B, Liu J. Building and Application of Delayed Coking Structure-Oriented Lumping Model. *Industrial & Engineering Chemistry Research*. 2012;51(10):3923-3931.
10. Wei W, Bennett CA, Tanaka R, Hou G, Klein MT. Detailed kinetic models for catalytic reforming. *Fuel Processing Technology*. 2008;89(4):344-349.
11. Dente M, Ranzi E, Goossens AG. Detailed prediction of olefin yields from hydrocarbon pyrolysis through a fundamental simulation model (SPYRO). *Computers & Chemical Engineering*. 1979;3(1-4):61-75.
12. Nguyen TT, Teratani S, Tanaka R, Endo A, Hirao M. Development of a structure-based lumping kinetic model for light gas oil hydrodesulfurization. *Energy & Fuels*. 2017;31(5):5673-5681.
13. Alvarez-Majmutov A, Chen J. Stochastic modeling and simulation approach for industrial fixed-bed hydrocrackers. *Industrial & Engineering Chemistry Research*. 2017;56(24):6926-6938.
14. Standl S, Kirchberger FM, Kühlewind T, et al. Single-event kinetic model for methanol-to-olefins (MTO) over ZSM-5: Fundamental kinetics for the olefin co-feed reactivity. *Chemical Engineering Journal*. 2020;402:126023.
15. Vinu R, Broadbelt LJ. A mechanistic model of fast pyrolysis of glucose-based carbohydrates to predict bio-oil composition. *Energy & Environmental Science*. 2012;5(12):9808-9826.
16. Van Geem KM, Reyniers M-F, Marin GB, Song J, Green WH, Matheu DM. Automatic reaction network generation using RMG for steam cracking of n-hexane. *AIChE Journal*. 2006;52(2):718-730.
17. Froment GF. Single event kinetic modeling of complex catalytic processes. *Catalysis Reviews*.

- 2005;47(1):83-124.
18. Broadbelt LJ, Stark SM, Klein MT. Computer Generated Pyrolysis Modeling: On-the-Fly Generation of Species, Reactions, and Rates. *Industrial & Engineering Chemistry Research*. 1994;33(4):790-799.
 19. Wei W, Bennett CA, Tanaka R, Hou G, Klein MT, Klein MT. Computer aided kinetic modeling with KMT and KME. *Fuel Processing Technology*. 2008;89(4):350-363.
 20. Watson BA, Klein MT. Mechanistic Modeling of n-Heptane Cracking on HZSM-5. *Industrial & Engineering Chemistry Research*. 1996;35(5):1506-1516.
 21. Watson BA, Klein MT. Mechanistic Modeling of a 1-Phenyloctane/n-Hexadecane Mixture on Rare Earth Y Zeolite. *Industrial & Engineering Chemistry Research*. 1997;36(8):2954-2963.
 22. Moustafa TM, Froment GF. Kinetic Modeling of Coke Formation and Deactivation in the Catalytic Cracking of Vacuum Gas Oil. *Industrial & Engineering Chemistry Research*. 2003;42(1):14-25.
 23. Quann RJ, Jaffe SB. Structure-oriented lumping: describing the chemistry of complex hydrocarbon mixtures. *Industrial & Engineering Chemistry Research*. 1992;31(11):2483-2497.
 24. Quann RJ, Jaffe SB. Building useful models of complex reaction systems in petroleum refining. *Chemical Engineering Science*. 1996;51(10):1615-1635.
 25. Mi Saine Aye M, Zhang N. A novel methodology in transforming bulk properties of refining streams into molecular information. *Chemical Engineering Science*. 2005;60(23):6702-6717.
 26. Gomez-Prado J, Zhang N, Theodoropoulos C. Characterisation of heavy petroleum fractions using modified molecular-type homologous series (MTHS) representation. *Energy*. 2008;33(6):974-987.
 27. Christensen G, Apelian MR, Hickey KJ, Jaffe SB. Future directions in modeling the FCC process: An emphasis on product quality. *Chemical Engineering Science*. 1999;54(13):2753-2764.
 28. Qin X, Liu J, Wang C, et al. Molecular level analysis on performance of diameter expanding reactor to improve gasoline quality in FCC process. *Fuel*. 2021;290:119978.
 29. Dewachtere NV, Santaella F, Froment GF. Application of a Single-Event Kinetic Model in the Simulation of an Industrial Riser Reactor for the Catalytic Cracking of Vacuum Gas Oil. *Chemical Engineering Science*. 1999;54(15):3653-3660.
 30. Liu J, Chen H, Pi Z, Liu Y, Sun H, Shen B. Molecular-Level-Process Model with Feedback of the Heat Effects on a Complex Reaction Network in a Fluidized Catalytic Cracking Process. *Industrial & Engineering Chemistry Research*. 2017;56(13):3568-3577.
 31. Kunii D, Levenspiel O. *Fluidization engineering*: Butterworth-Heinemann; 1991.
 32. Faltsi-Saravelou O, Vasalos I. FBSim: A model for fluidized bed simulation—I. Dynamic modeling of an adiabatic reacting system of small gas fluidized particles. *Computers & chemical engineering*. 1991;15(9):639-646.
 33. Zhang Y, Lu C, Li T. A practical countercurrent fluid catalytic cracking regenerator model for in situ operation optimization. *AIChE journal*. 2012;58(9):2770-2784.
 34. Ali H, Rohani S. Dynamic modeling and simulation of a riser-type fluid catalytic cracking unit. *Chemical Engineering & Technology: Industrial Chemistry-Plant Equipment-Process Engineering-Biotechnology*. 1997;20(2):118-130.
 35. Han I-S, Chung C-B. Dynamic modeling and simulation of a fluidized catalytic cracking process. Part I: Process modeling. *Chemical Engineering Science*. 2001;56(5):1951-1971.
 36. Han I-S, Chung C-B. Dynamic modeling and simulation of a fluidized catalytic cracking process. Part II: Property estimation and simulation. *Chemical Engineering Science*. 2001;56(5):1973-1990.
 37. Zhou X, Yang Q, Yang S, et al. One-step leap in achieving oil-to-chemicals by using a two-stage riser reactor: Molecular-level process model and multi-objective optimization strategy. *Chemical*

- Engineering Journal*. 2022;444:136684.
38. Dasila PK, Choudhury IR, Singh S, Rajagopal S, Chopra SJ, Saraf DN. Simulation of an industrial fluid catalytic cracking riser reactor using a novel 10-lump kinetic model and some parametric sensitivity studies. *Industrial & Engineering Chemistry Research*. 2014;53(51):19660-19670.
 39. Feng S, Cui C, Li K, et al. Molecular composition modelling of petroleum fractions based on a hybrid structural unit and bond-electron matrix (SU-BEM) framework. *Chemical Engineering Science*. 2019;201:145-156.
 40. Cui, Chen, Billa, et al. Molecular Representation of the Petroleum Gasoline Fraction. *Energy & Fuels*. 2018.
 41. Guan D, Chen Z, Chen X, et al. Molecular-level heavy petroleum hydrotreating modeling and comparison with high-resolution mass spectrometry. *Fuel*. 2021;297:120792.
 42. Chen Z, Feng S, Zhang L, et al. Molecular-level kinetic modeling of heavy oil fluid catalytic cracking process based on hybrid structural unit and bond-electron matrix. *AIChE Journal*. 2021;67(1):e17027.
 43. Yang M, Zhang L, Wang G, et al. Fischer-Tropsch wax catalytic cracking for the production of low olefin and high octane number gasoline: Experiment and molecular level kinetic modeling study. *Fuel*. 2021;303:121226.
 44. Weisz PB, Goodwin R. Combustion of carbonaceous deposits within porous catalyst particles I. Diffusion-controlled kinetics. *Journal of Catalysis*. 1963;2(5):397-404.
 45. Weisz PB. Combustion of carbonaceous deposits within porous catalyst particles: III. The CO₂/CO product ratio. *Journal of Catalysis*. 1966;6(3):425-430.
 46. Weisz PB, Goodwin RB. Combustion of carbonaceous deposits within porous catalyst particles: II. Intrinsic burning rate. *Journal of Catalysis*. 1966;6(2):227-236.
 47. Alwahabi SM, Froment GF. Conceptual reactor design for the methanol-to-olefins process on SAPO-34. *Industrial & engineering chemistry research*. 2004;43(17):5112-5122.
 48. Chen Z, Yao X, Guan D, Zhao S, Zhang L, Xu C. Vacuum residue coking process simulation using molecular-level kinetic model coupled with vapor-liquid phase separation. *Chinese Journal of Chemical Engineering*. 2022;41:301-310.
 49. Chen Z, Guan D, Zhang X, et al. A mass-temperature decoupled discretization strategy for large-scale molecular-level kinetic model. *Chemical Engineering Science*. 2022;249:117348.
 50. Chen Z, Feng S, Zhang L, et al. Molecular-level kinetic modelling of fluid catalytic cracking slurry oil hydrotreating. *Chemical Engineering Science*. 2019;195:619-630.
 51. Souza J, Vargas J, Von Meien O, Martignoni W, Amico S. A two-dimensional model for simulation, control, and optimization of FCC risers. *AIChE journal*. 2006;52(5):1895-1905.
 52. Gao J, Xu C, Lin S, Yang G, Guo Y. Advanced model for turbulent gas–solid flow and reaction in FCC riser reactors. *AIChE Journal*. 1999;45(5):1095-1113.

Figure

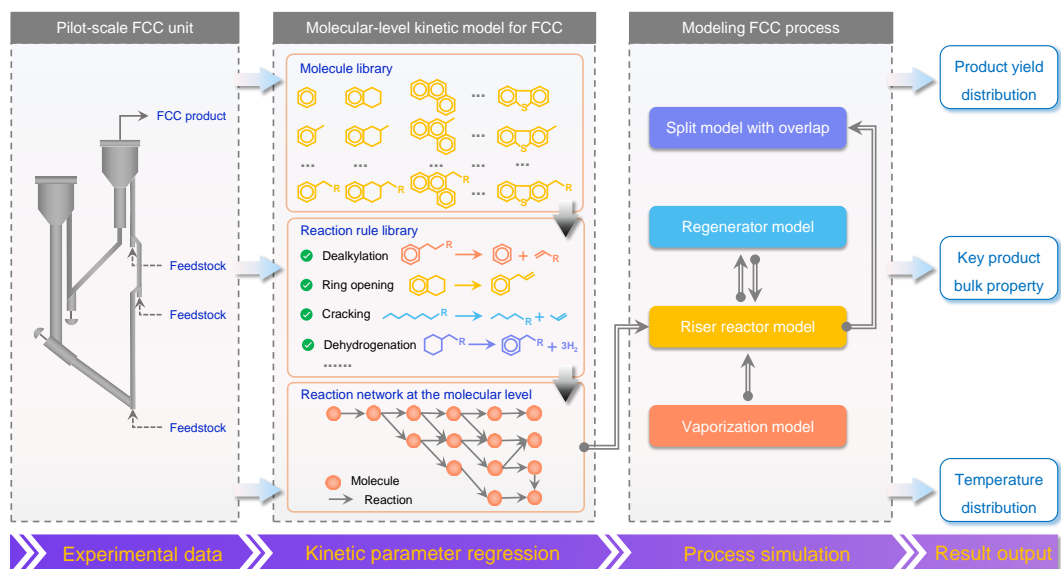


Figure 1. Overview of the heavy oil FCC process simulation at the molecular level

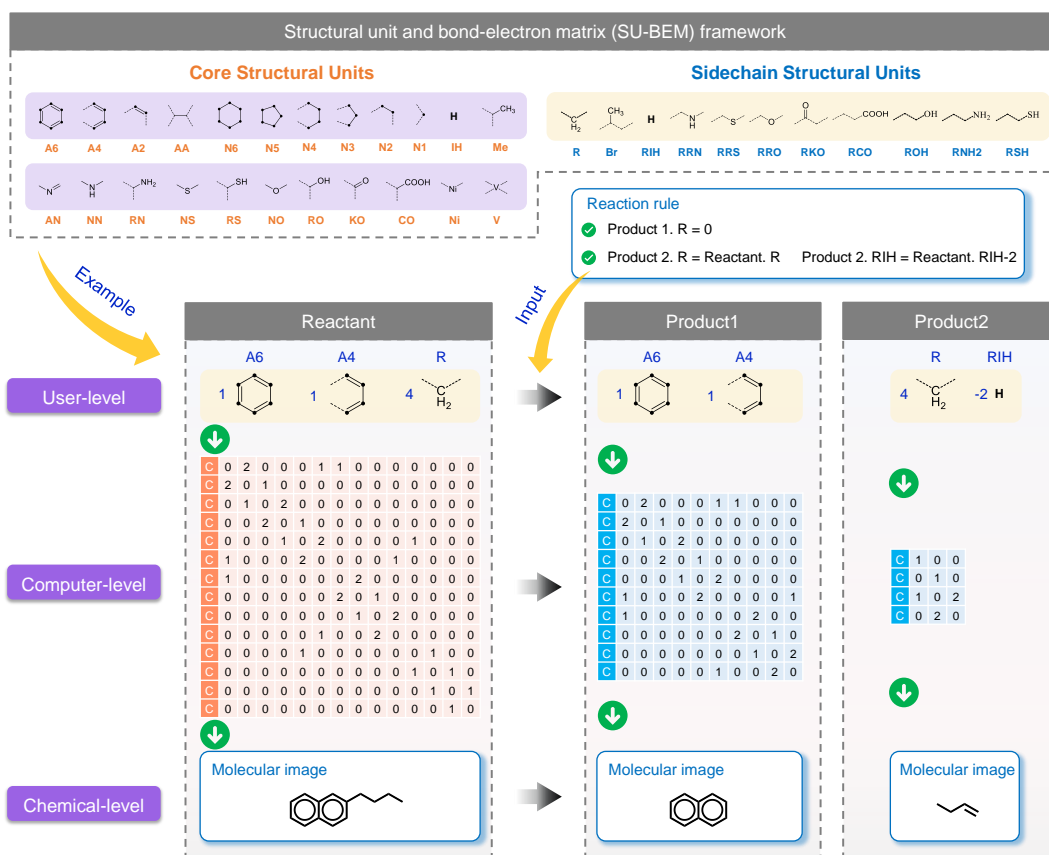


Figure 2. Structural units in the SU-BEM framework and examples of reaction generation based on SU-BEM

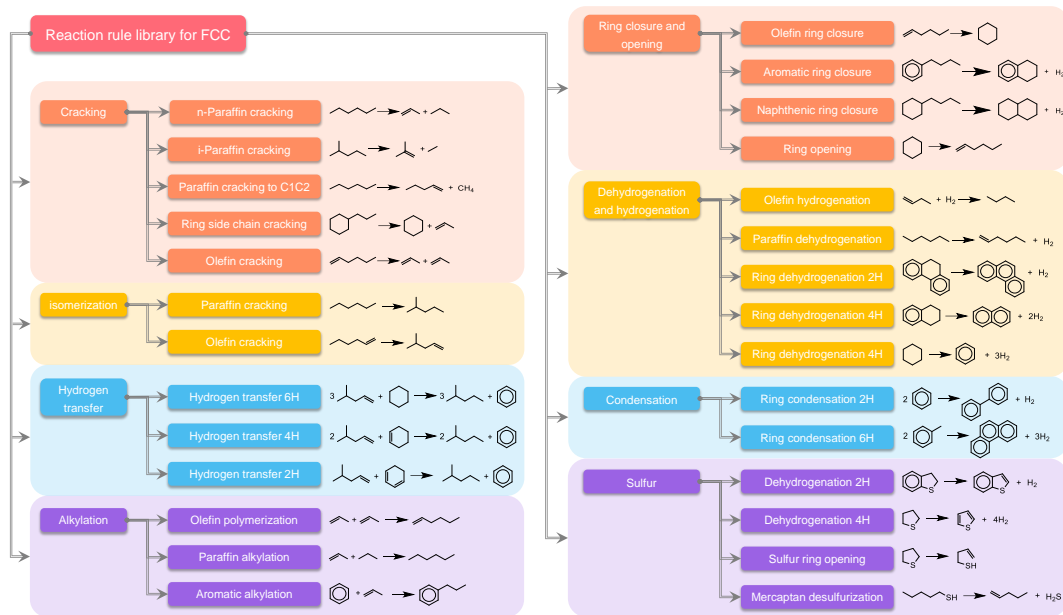


Figure 3. Reaction rule library for FCC process at the pathway level

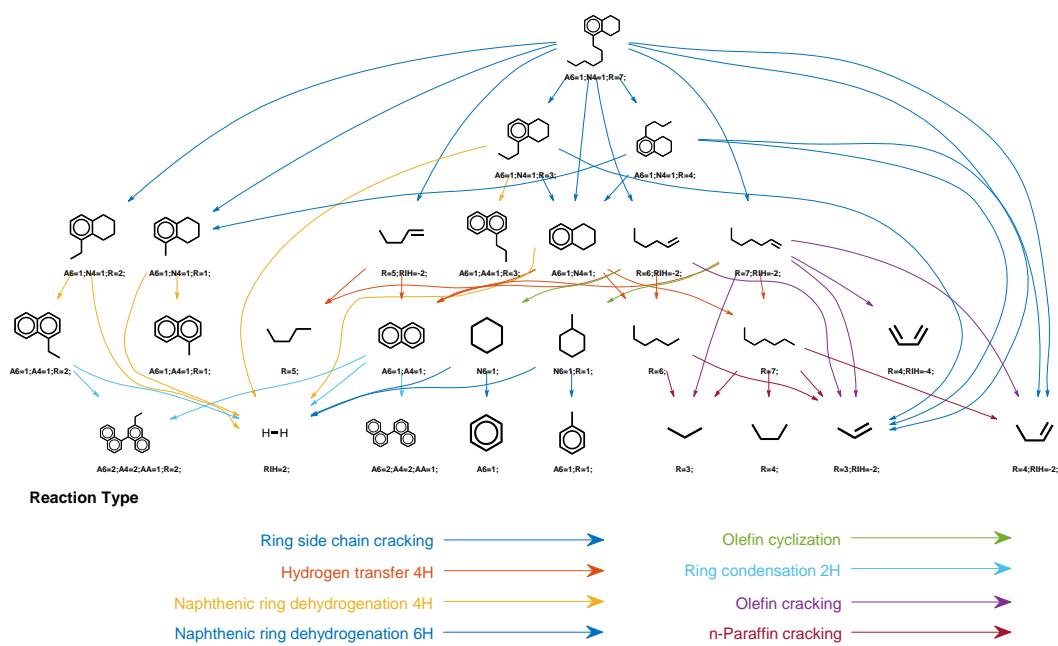


Figure 4. The reaction network of C7-tetrahydronaphthalene FCC

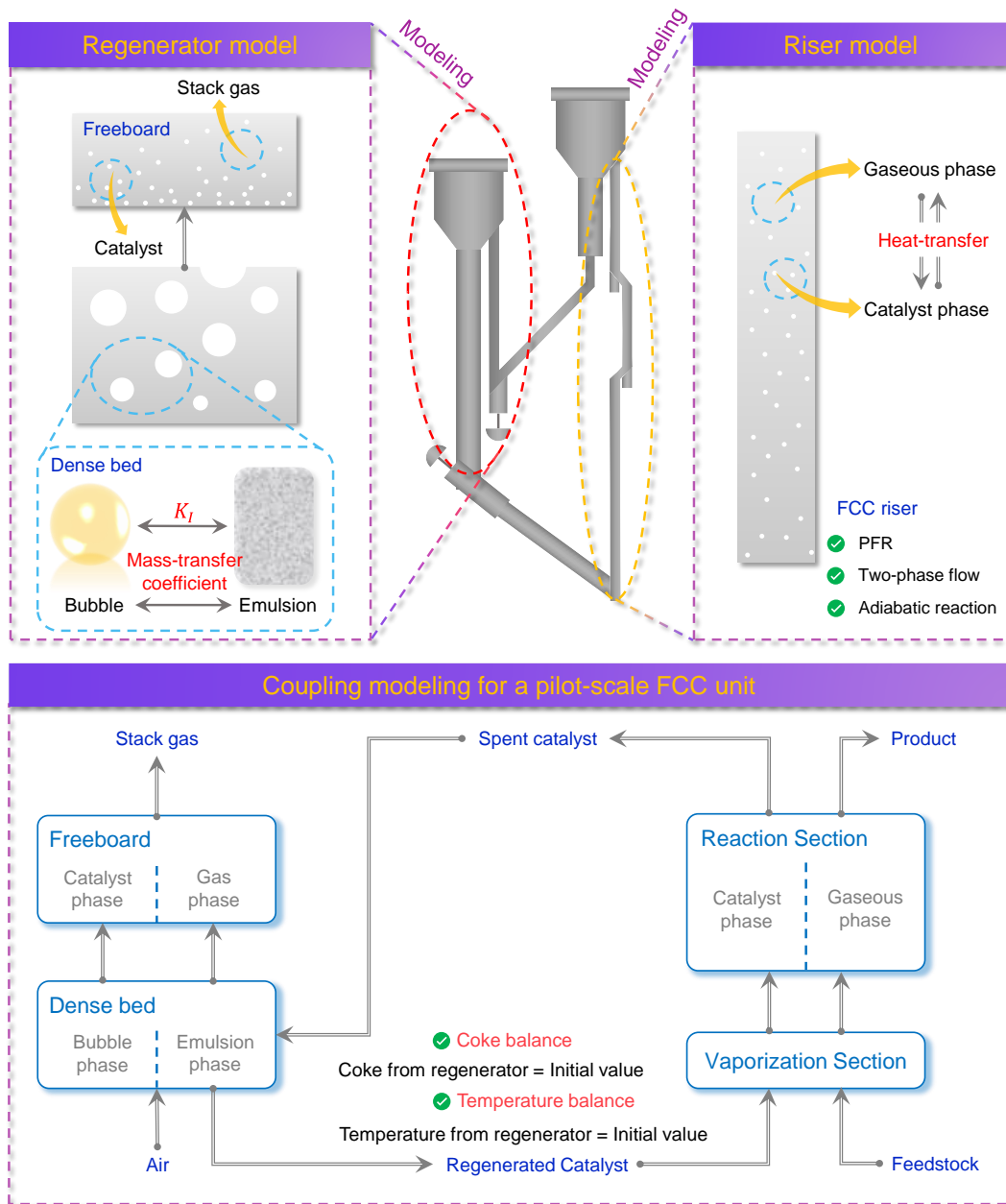


Figure 5. Experimental scheme and modeling for FCC pilot plant

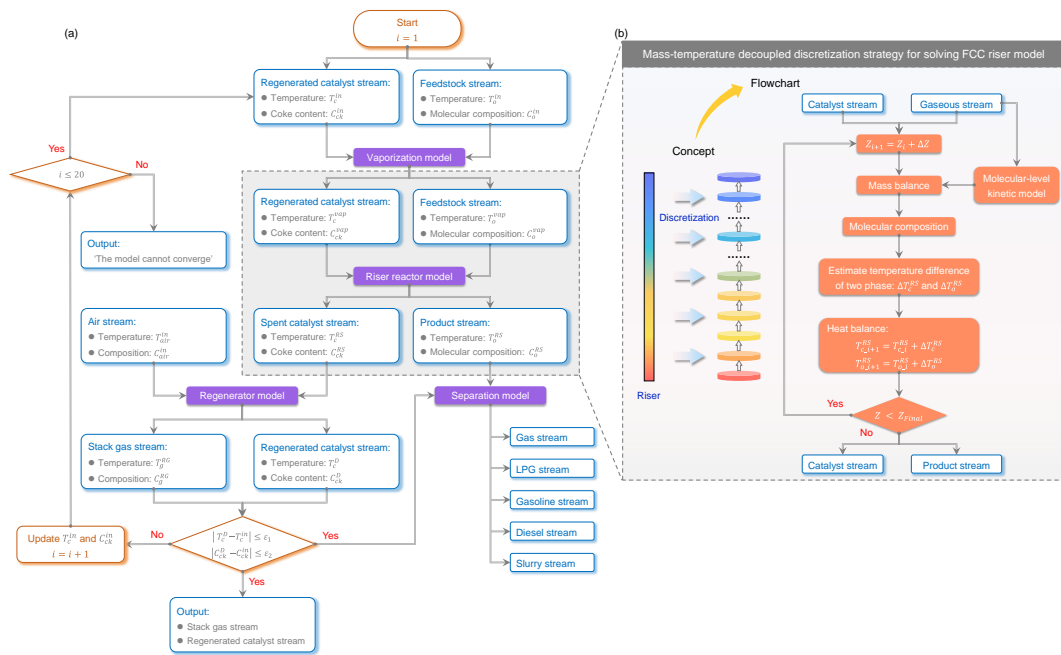


Figure 6. Iteration scheme of FCC process simulation for convergence

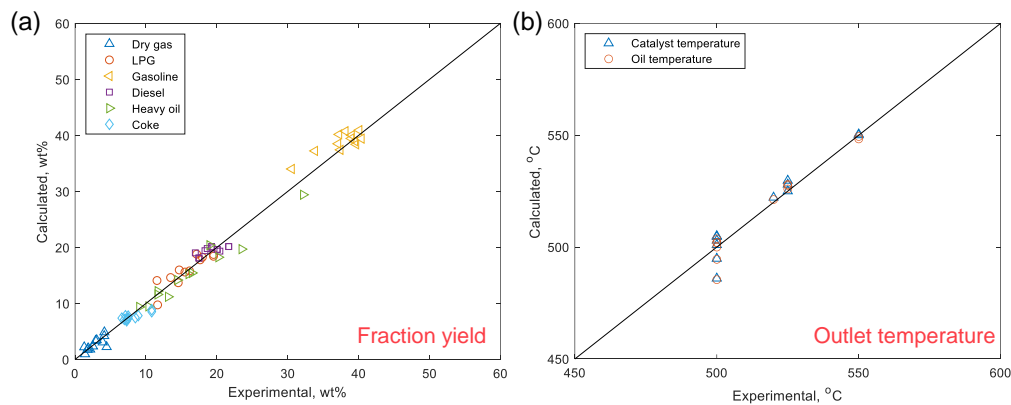


Figure 7. Parity plots comparing experimental and calculated data for heavy oil FCC. (a) fraction yield; (b) outlet temperature of the riser

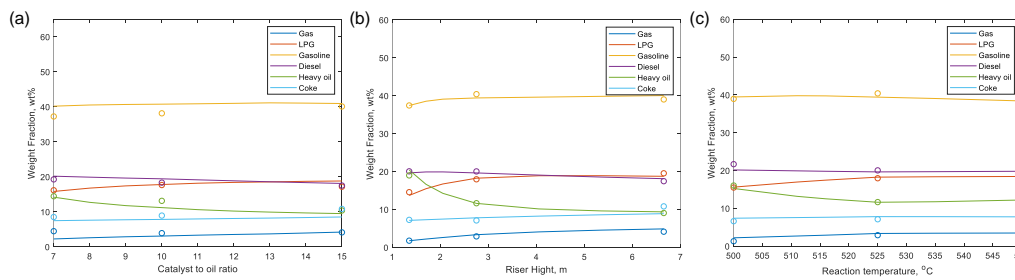


Figure 8. The effect of reaction conditions on the fraction yield for FCC. (a) CTO; (b) Riser height; (c) Reaction temperature.

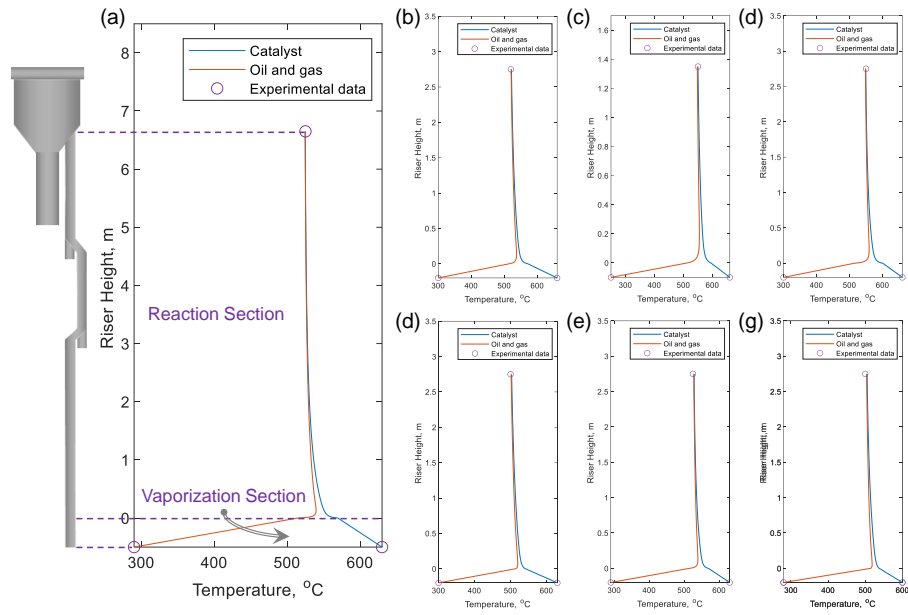


Figure 9. Temperature of catalyst and oil along the riser. (a) test 11; (b) test 3; (c) test 4; (d) test 5; (e) test 7; (f) test 10; (g) test 12.

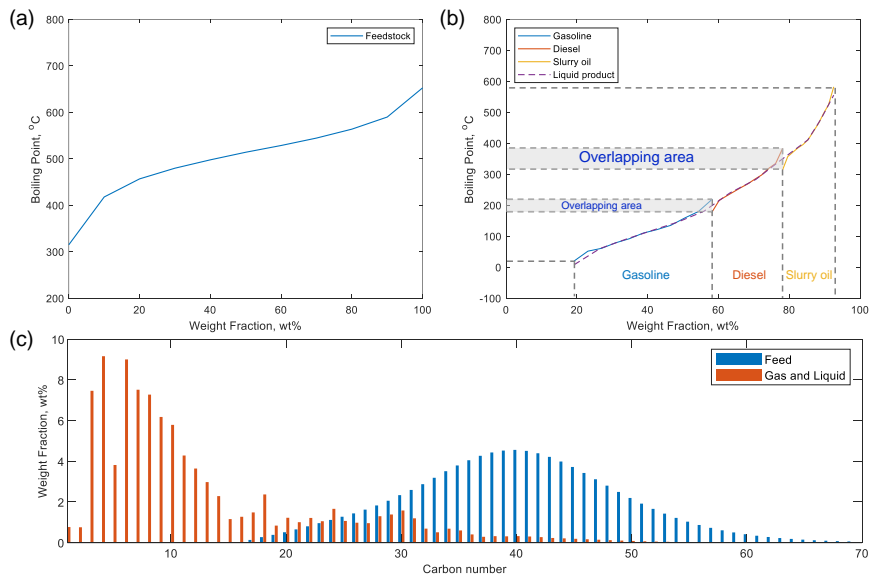


Figure 10. The calculated result of distillation curve for liquid product and carbon number distribution. (a) Distillation curve for feedstock; (b) Distillation curve for liquid; (c) Carbon number distribution for the feedstock and product.

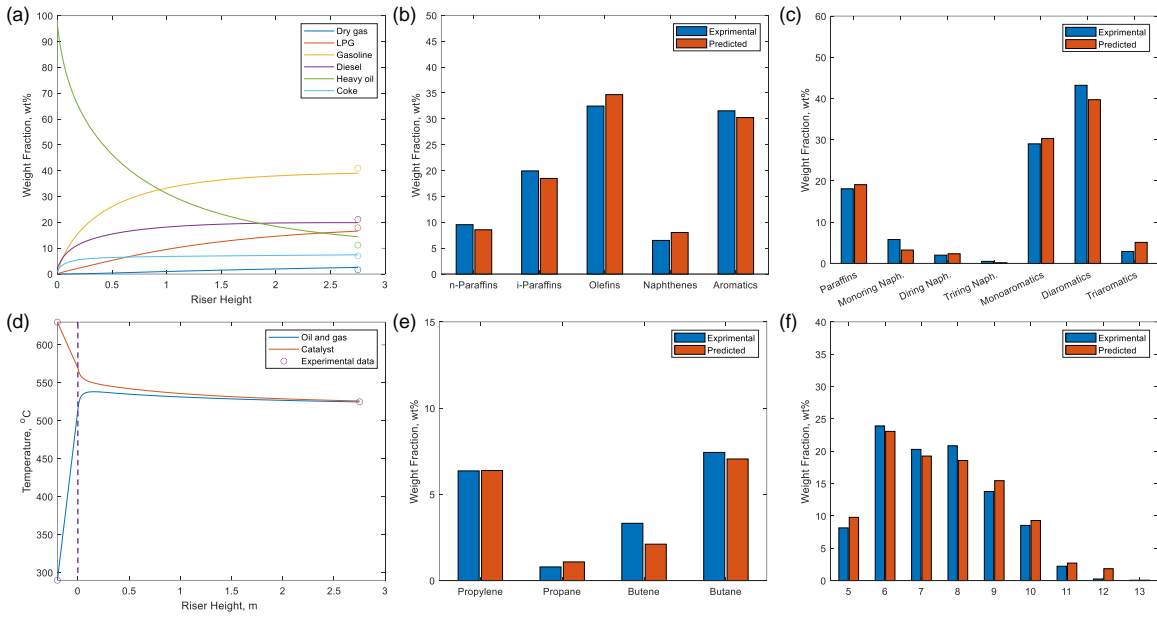


Figure 11. Comparison of experimental and predicted value for FCC process simulation. (a) product yield; (b) Gasoline composition; (c) Diesel composition; (d) Reaction temperature; (e) LPG composition; (f) Carbon number distribution for gasoline.

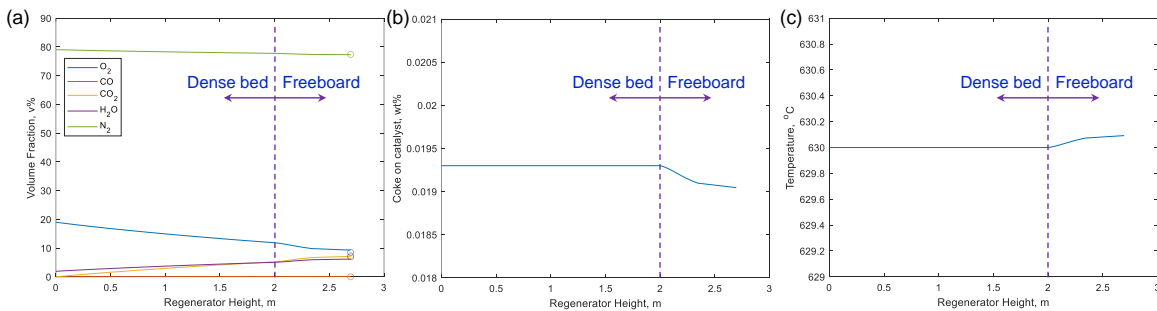


Figure 12. Calculate results for the regenerator. (a) stack gas composition; (b) coke distribution; (c) temperature distribution.

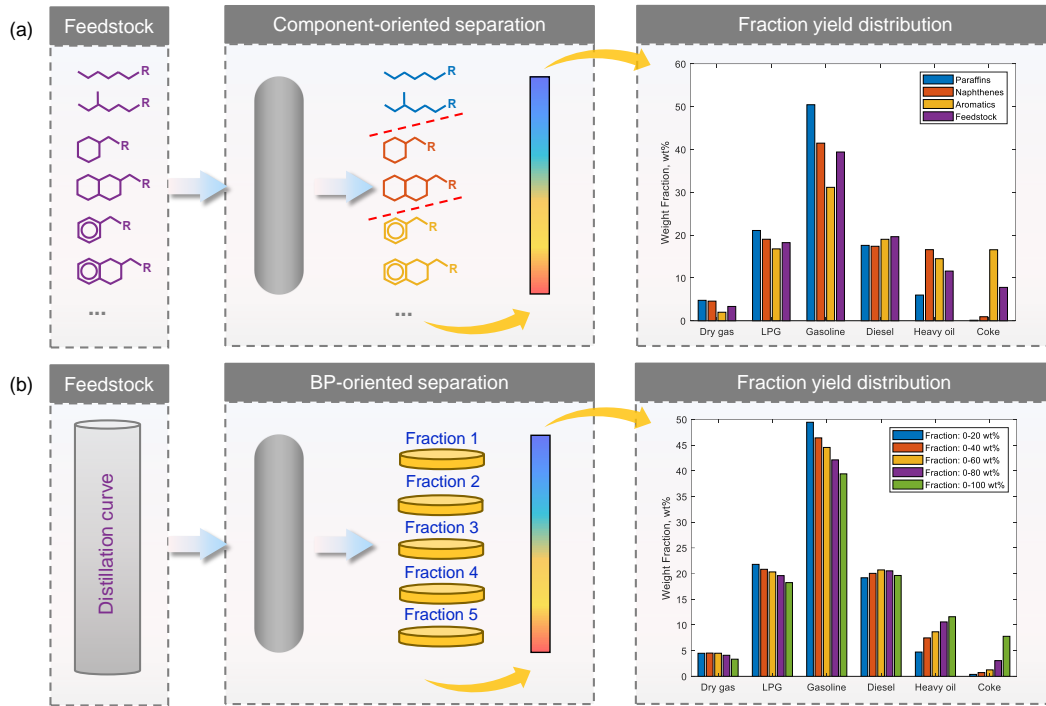


Figure 13. The effect of feedstock composition on the fraction yield for FCC. (a) Component; (b) Boiling point.

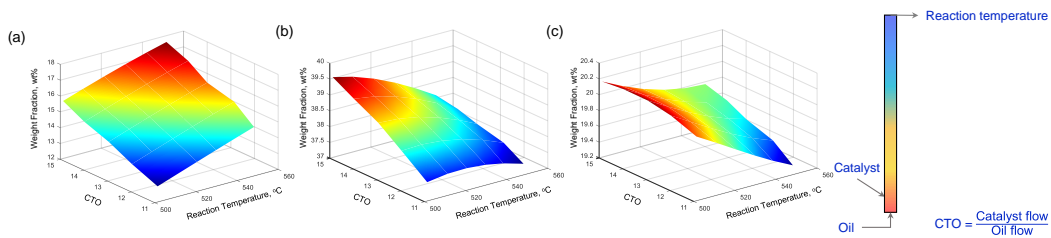


Figure 14. The effect of the process conditions on the key fraction yield. (a) LPG; (b) Gasoline; (c) Diesel.

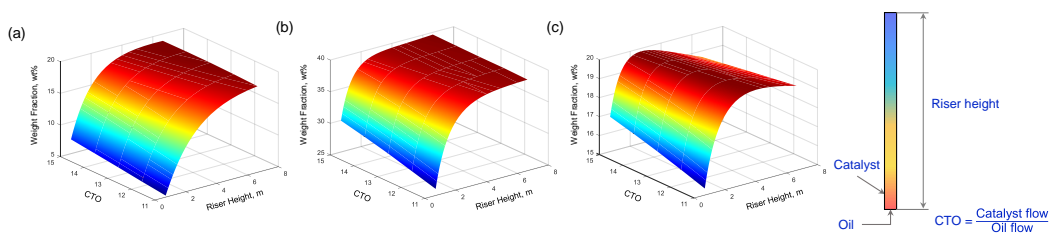


Figure 15. The effect of riser height on the key fraction yield. (a) LPG; (b) Gasoline; (c) Diesel.

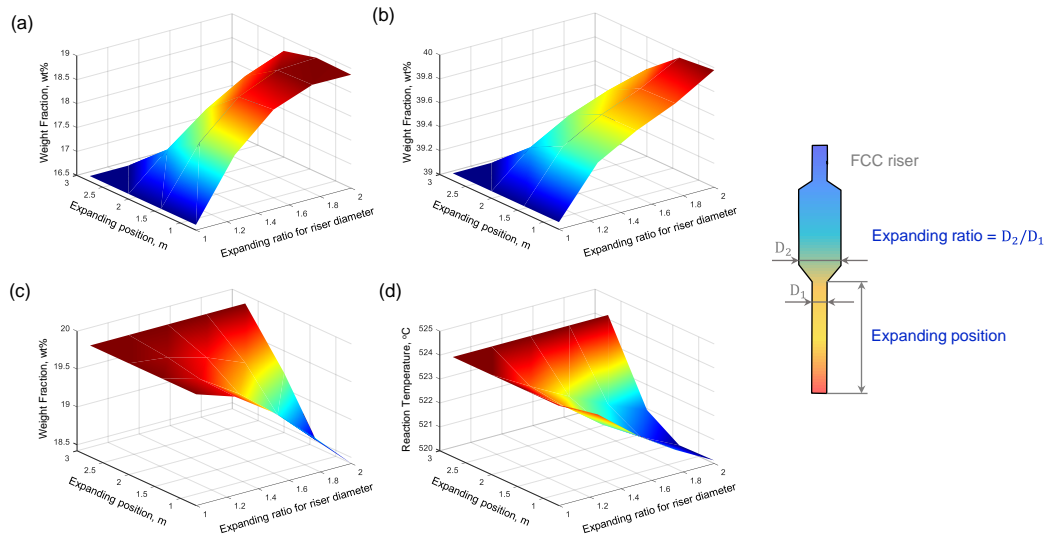


Figure 16. The effect of riser structure on the key fraction yield. (a) LPG; (b) Gasoline; (c) Diesel; (d) Outlet temperature of riser.

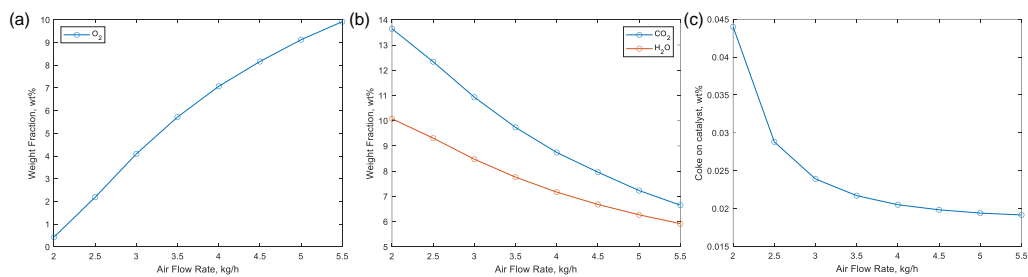


Figure 17. The effect of air flow rate on the stack gas and coke. (a) O₂; (b) CO₂ and H₂O; (c) Coke on the catalyst.